



OPEN

## Characterization of the temporal stability of ToM and pain functional brain networks carry distinct developmental signatures during naturalistic viewing

Km Bhavna<sup>1</sup>, Niniva Ghosh<sup>2</sup>, Romi Banerjee<sup>1,2</sup> & Dipanjan Roy<sup>1,2✉</sup>

A temporally stable functional brain network pattern among coordinated brain regions is fundamental to stimulus selectivity and functional specificity during the critical period of brain development. Brain networks that are recruited in time to process internal states of others' bodies (like hunger and pain) versus internal mental states (like beliefs, desires, and emotions) of others' minds allow us to ask whether a quantitative characterization of the stability of these networks carries meaning during early development and constrain cognition in a specific way. Previous research provides critical insight into the early development of the theory-of-mind (ToM) network and its segregation from the Pain network throughout normal development using functional connectivity. However, a quantitative characterization of the temporal stability of ToM networks from early childhood to adulthood remains unexplored. In this work, reusing a large sample of children ( $n = 122$ , 3–12 years) and adults ( $n = 33$ ) dataset that is available on the OpenfMRI database under the accession number ds000228, we addressed this question based on their fMRI data during a short and engaging naturalistic movie-watching task. The movie highlights the characters' bodily sensations (often pain) and mental states (beliefs, desires, emotions), and is a feasible experiment for young children. Our results tracked the change in temporal stability using an unsupervised characterization of ToM and Pain networks DFC patterns using Angular and Mahalanobis distances between dominant dynamic functional connectivity subspaces. Our findings reveal that both ToM and Pain networks exhibit lower temporal stability as early as 3-years and gradually stabilize by 5-years, which continues till adolescence and late adulthood (often sharing similarity with adult DFC stability patterns). Furthermore, we find that the temporal stability of ToM brain networks is associated with the performance of participants in the false belief task to access mentalization at an early age. Interestingly, higher temporal stability is associated with the pass group, and similarly, moderate and low temporal stability are associated with the inconsistent group and the fail group. Our findings open an avenue for applying the temporal stability of large-scale functional brain networks during cortical development to act as a biomarker for multiple developmental disorders concerning impairment and discontinuity in the neural basis of social cognition.

**Keywords** Theory-of-mind (ToM), Pain networks, Angular distance, Mahalanobis distance, Dynamic functional connectivity (DFC)

Theory-of-mind (ToM) is an evolving ability that significantly impacts human learning and cognition and is highlighted in 1970 by Premack and Woodruff<sup>1</sup>. The ToM ability allows individuals to comprehend other people's aims, ambitions, and thinking that differ from their own<sup>2</sup>. Recent studies have primarily focused on understanding the development of ToM functions from the preschool age group and its association with middle childhood and early adolescence and characterized individual differences<sup>3</sup>. According to the literature, children develop the ability to understand aim and intention and predict another person's actions in false belief task

<sup>1</sup>Department of Computer Science and Engineering, Indian Institute of Technology, Jodhpur 342030, Rajasthan, India. <sup>2</sup>School of AIDE, Indian Institute of Technology, Centre for Brain Science Application, Jodhpur 342030, Rajasthan, India. ✉email: droy@iitj.ac.in

paradigms by the age of 4 years<sup>3–6</sup>. Hence, children's performance in explicit false belief tasks could index an important milestone in understanding concepts during ToM development, as theories of others' internal states are dramatically altered by insight into the representational nature of mental states. Analyzing the early age group data allows us to examine the development of the ToM network and re-examine the literature about children's ToM functional brain networks during naturalistic movie-watching tasks. Using naturalistic stimuli enables us to identify age-specific patterns in brain connectivity and how these patterns change as children grow, helping us track developmental trajectories in neural connectivity and their implications for cognitive processing. The human brain is a collection of massive functional modules that become more distinct during development from childhood to adolescence, i.e., connectivity within modules increases as we grow from childhood to adolescence, and connectivity between modules decreases<sup>7–10</sup>. Therefore, previous studies have focused on functional connectivity measures within and between ToM and pain brain networks to address children's early developmental differences and functional specialization from 3 to 12 years and, subsequently, employed within and between-network functional connectivity measures to relate to performance in explicit false belief reasoning tasks<sup>4</sup>. Moreover, previous studies have reported a striking division between regions responding preferentially to internal states of others' bodies (like hunger, pain, and mental states) versus internal states (like beliefs and desires) of others' minds, suggesting a division of labor and early segregation into functionally specialized brain regions<sup>4,11</sup>. Recently, dynamic functional connectivity (DFC) and temporal stability of DFC have emerged as a major topic in the resting-state BOLD functional magnetic resonance imaging (fMRI) literature<sup>12–14</sup>. DFC captures fluctuation in temporal scale of minutes that contain meaningful information<sup>14,15</sup>. While the participants are experiencing naturalistic stimuli, fluctuations and stochasticity inherent in temporal dynamics of DFC may be crucial in shaping slow neuronal dynamics of ToM brain regions; on the contrary, a stable representation of temporal dynamics and corresponding stability of FC patterns over time are crucial for functional development of the cortex<sup>12</sup>. In this context, which are the key contributors that sculpt the stability of dynamic FC patterns during tasks, and how they associate with different salient stimuli present in the movie clips (e.g., hunger, pain, and internal states like belief and desires) are vital questions to address. To this end, systematic quantitative characterization of the temporal stability measure that captures the variability or consistency of neural activity patterns over time (i.e., less temporal stability means more variability and vice-versa) and coordination between functionally specialized brain regions across neurodevelopment remain unexplored. Previous studies investigated the differences in temporal stability of functional architecture in the resting states of patients with neurological disorders and healthy controls and examined the effects of various activities<sup>12–14</sup>. The studies also demonstrated that variable alterations in the functional architecture of the default mode network (DMN), visual and subcortical brain areas, which were specific to some neurological disorders (e.g., ADHD, schizophrenia, and autism spectrum disorder)<sup>12–14</sup>. Therefore, existing neuroimaging studies leave a gap in addressing fundamental questions of interest concerning temporal stability in the early stages of development in the ToM functional brain networks and their association with behavior.

Recent evidence suggests that during ToM-related tasks, neural activation is found predominantly in the Bilateral Temporoparietal Junction (Left TPJ and Right TPJ), Medial Prefrontal Cortex, and Posterior Cingulate Cortex using fMRI data; however, it remains unknown at which stage of neurodevelopment the temporal stability of these regions undergoes alterations<sup>11</sup>. Moreover, there are no existing studies that quantify whether the temporal stability of social brain regions of ToM and Pain (sensory) networks carry distinct or overlapping signatures during naturalistic stimulus processing in children during development and whether the pattern of temporal stability indicates the successful development of ToM reasoning ability thus far. Secondly, whether the temporal stability patterns of social brain regions of ToM in 3–12 years could be associated with the performance in false belief reasoning tasks remains least understood<sup>4,5</sup>. According to our hypothesis, the aim of the present study is twofold: (1) to precisely characterize the temporal stability of ToM and Pain brain networks and age-associated differences in the stability and fluctuations from the early childhood stage to adolescence using a recently proposed novel unsupervised approach; (2) to identify whether temporal stability of ToM functional brain networks could be associated with success or failure in explicit false belief task performance in children and adults. Our findings contribute significantly to the ongoing understanding of the neural dynamics at the early developmental stage by focusing on ToM functional brain networks and the potential utility of their temporal stability as an associated measure with individual differences in false belief task performance.

The article is organized as follows: firstly, to test our hypothesis, we used an early childhood dataset comprising 122 participants (3–12 years age range) with 33 adult controls (total number of participants = 155) passively viewing a short, animated movie that included events evoking the mental states and physical bodily sensations of the clip characters while undergoing fMRI. A recent study has validated this movie, which activates ToM brain regions and the pain regions<sup>4</sup>. To check how temporal stability differs between ToM and pain scenes and evolves in both cases upon aging, we used a data-driven unsupervised approach to capture high-dimensional dynamic functional connectivity (DFC) via low-dimensional patterns and subsequent estimation of temporal stability using quantitative metrics. The reason for using temporal stability instead of the traditional approaches was its ability to capture dynamic changes over time (even in a tiny instance), individual variability, and developmental trajectories. We use Angular and Mahalanobis distances to identify the ToM and Pain network temporal stability when movie stimuli/clips contain internal activation of mental and physical states activating brain networks at specific moments in time. We have conducted the following analysis to address core questions regarding the temporal stability of functional brain networks (ToM and Pain) involved in representing internal mental and physical states. The brain regions associated with ToM and pain networks have been selected based on a previous study that reported 12 brain regions (refer to Table 1)<sup>4,16,17</sup>. ToM brain regions include bilateral temporoparietal junction, precuneus, and middle, dorso- and ventromedial prefrontal cortices. The pain network comprises brain regions recruited when perceiving the physical pain and bodily sensations of others: bilateral medial frontal gyrus, insular cortex, secondary sensory cortex, and dorsal anterior middle cingulate cortex. As in

ToM regions			Pain regions		
Sr. no.	ROIs	MNI coordinates (X,Y,Z)	Sr. no.	ROIs	MNI coordinates (X,Y,Z)
1	Posterior cingulate cortex (PCC)	0, -52, 18	1	Right middle frontal gyrus (RMFC)	36, 38, 40
2	Left temporoparietal junction (LTPJ)	-46, -68, 32	2	Left middle frontal gyrus (LMFC)	-36, 38, 40
3	Right temporoparietal junction (RTPJ)	46, -68, 32	3	Left inferior insula (LII)	-40, 22, 0
4	Ventromedial prefrontal cortex (vmPFC)	4, 48, -4	4	Right inferior insula (RII)	39, 23, -4
5	Precuneus	0, -49, 40	5	Left secondary sensory cortex (LSSC)	-39, -15, 18
6	Dorsomedial prefrontal cortex (dmPFC)	-10, 58, 24	6	Right secondary sensory cortex (RSSC)	39, -15, 18

**Table 1.** Table shows selected ToM and pain brain regions and corresponding MNI coordinated for extracting time-series signal.

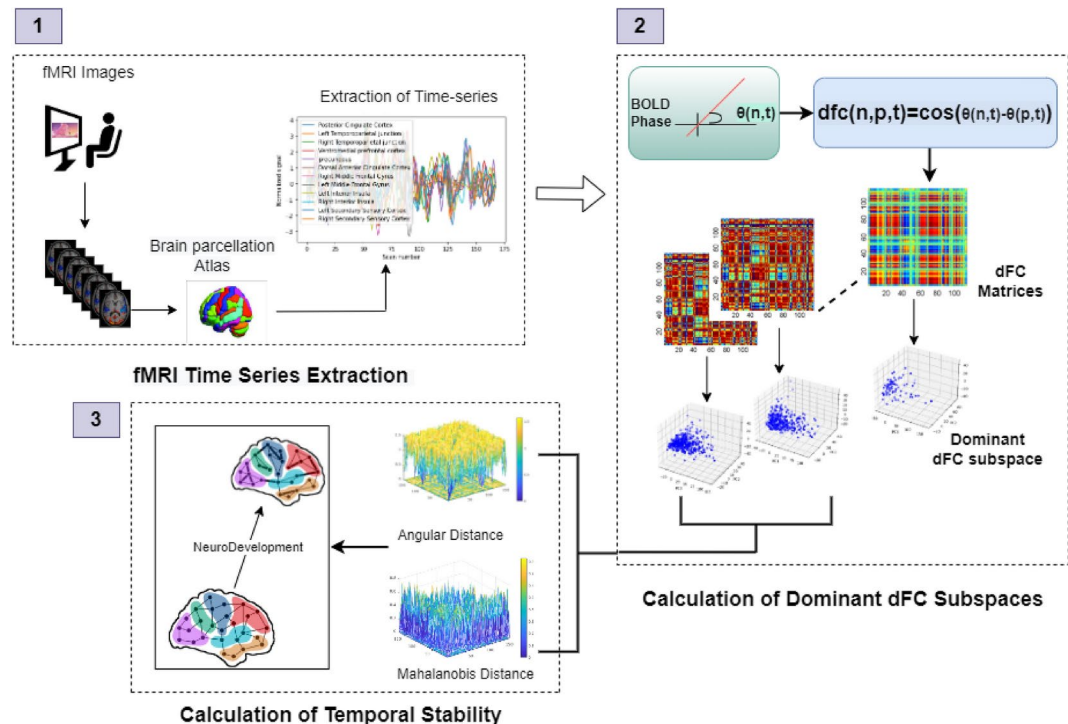


**Figure 1.** Illustrative overview of the proposed architecture for identifying age at which ToM and pain networks are getting reasonable temporal stability and how it is associated with behavioral scores of the false belief task. The paper's contribution is as follows: (1) Data collection during naturalistic movie watching and extraction of time-series from ToM and pain networks, (2) calculation of DFC matrices and then calculation of dominant DFC sub-spaces, and (3) Calculation of Angular distance and Mahalanobis distance using dominant DFC matrices, leading to temporal stability computations.

previous studies, we collapse these brain regions across specific functions and use ToM and pain networks as regions generally recruited for reasoning about others' internal mental and physical states. The contribution of the current study is as follows: (A) We used the dynamic functional connectivity (DFC) to quantify temporal stability using our previous approach<sup>14</sup> of functional brain networks in 3–12 years-old children. Subsequently, we estimated dominant DFC subspaces of ToM and Pain networks to quantify their separation at an early age. (B) To further capture ToM network temporal stability, we quantified differences between the dominant DFC subspaces using two distinct measures: (i) Angular Distance and (ii) Mahalanobis Distance. Our results suggest that ToM and Pain networks achieve considerable temporal stability by the age of 5 years. (C) Finally, we have tested whether the temporal stability of functional networks is associated with the performance of participants in false belief reasoning tasks based pass, fail, or give inconsistent groups, which is carried out by the 3–12 years-old participants outside the scanner. The analysis is performed for complete movie duration and additionally, we highlighted the temporal stability where movie clips evoked higher activation. Our finding grounded on derived temporal stability differences in functional brain networks during developmental age may aid in developing avenues to address questions related to distinct neural responses to others' minds and bodies that are present at a very early age and continue to develop after when children pass explicit false-belief tasks and throw fundamental insights into the development of ToM brain networks (refer to Fig. 1).

## Methods

### Participants and MRI preprocessing

In the current study, we analyzed a dataset of 155 early childhood to adult participants available on the OpenfMRI database under the accession number ds000228 and was originally collected by the Richardson et al. group<sup>4</sup>. The childhood group consisted of 122 participants aged 3–12-years (mean age = 6.7 years, SD = 2.3, 64 females), complemented by 33 adults (mean age = 24.8 years, SD = 5.3, 20 females)<sup>4</sup>. All the participants were from the local community and had submitted written consent from parent/guardian. The data were collected with approval from the Committee on the Use of Humans as Experimental Subjects (COUHES) at the Massachusetts Institute of Technology. Participants watched a sound-less short animated movie called “Partly Cloudy” for a total duration of 5.6 min, and the stimuli were validated to activate ToM and pain regions<sup>4,5,18</sup> (refer to Fig. 2). A 3-Tesla Siemens Tim Trio scanner at the Athinoula A. Martinos Imaging Center at MIT was used to collect whole-brain structural and functional MRI data<sup>19</sup>. Children under age 5-years used one of two custom 32-channel phased-array head coils made for younger ( $n = 3$ , M (s.d.) = 3.91 (0.42) years) or older ( $n = 28$ , M (s.d.) = 4.07 (0.42) years) children; all other participants used the standard Siemens 32-channel head coil<sup>4</sup>. With a factor of three for GRAPPA parallel imaging, 176 interleaved sagittal slices of 1 mm isotropic voxels were used to get T1-weighted structural images (FOV: 192 mm for child coils, 256 mm for adult coils). The whole brain was covered by 32 interleaved near-axial slices that were aligned with the anterior/posterior commissure and we used a gradient-echo EPI sequence sensitive to BOLD contrast to capture functional data (EPI factor: 64; TR: 2 s, TE: 30 ms, flip angle: 90°)<sup>4</sup>. All functional data were upsampled in normalized space to 2 mm isotropic voxels. Based on the participant’s head motion one TR back, prospective acquisition correction was used to modify the gradient locations.

fMRI data were analyzed using Matlab, R-written custom software, such as SPM8 (<http://www.fil.ion.ucl.ac.uk/spm>)<sup>20</sup>. Every participant’s anatomical image was standardized to the Montreal Neurological Institute (MNI) template, and functional images were registered to that image as the first image of the run<sup>21,22</sup>. This allowed us to directly compare responses between child and adult participants and utilize group regions of interest (ROIs) and hypothesis spaces generated in adult data sets. Every brain was visually registered to the MNI template, with attention paid to the cortical envelope and interior characteristics such as the main sulci and AC-PC. We smoothed all of the data using a 5 mm kernel Gaussian filter. By use of the ART toolbox ([https://www.nitrc.org/projects/artifact\\_detect/](https://www.nitrc.org/projects/artifact_detect/))<sup>23</sup>, artifact time points were defined as those for which the global signal fluctuated more than three standard deviations from the mean global signal or for which there was > 2 mm composite motion relative to the prior time point<sup>4,24,25</sup>. If one-third or more of the time points gathered were found to be artifact time points, individuals were removed from the sample. Both the number of artifact time points for the child and adult participants were substantially different (M (s.d.) = 10.5 (10.6) for the kid and 2.8 (4) for the adult; Welch two-sample t-test:  $t(137.7) = 6.49, p < 0.000001$ ). The no. of motion artifact timepoints among children

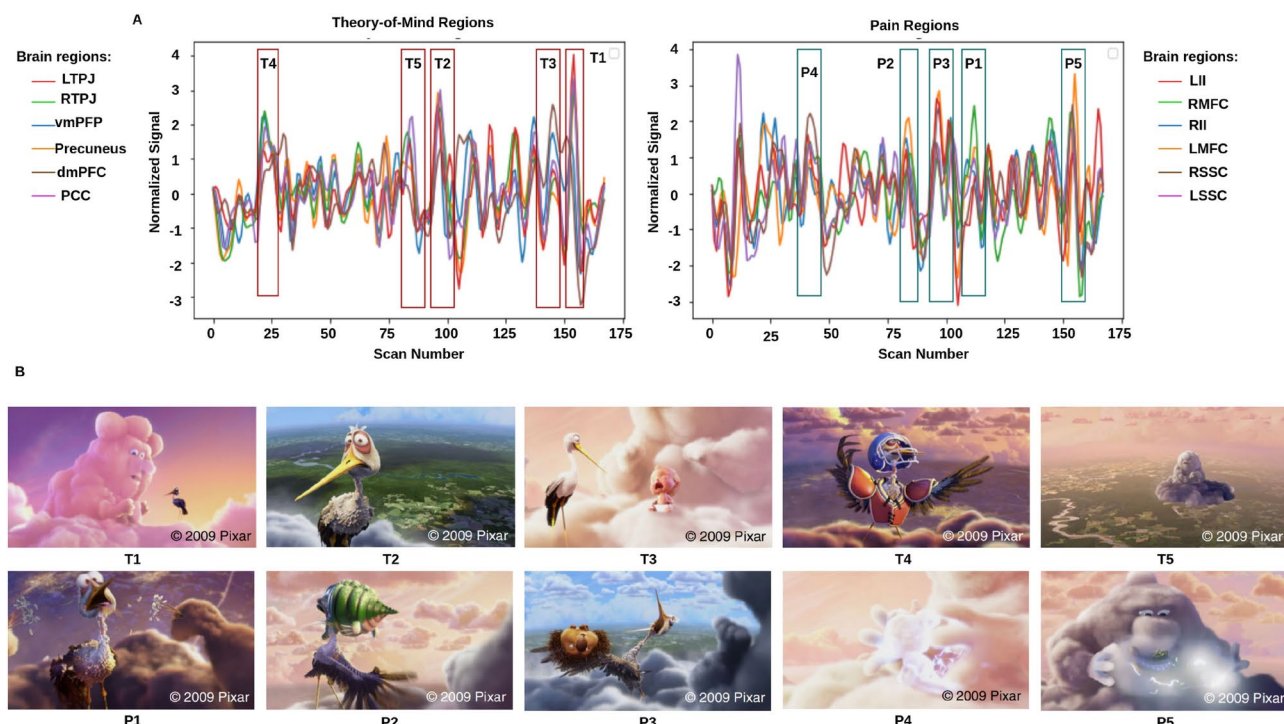


**Figure 2.** Movie demonstration: (A) response magnitude that evoked maximum activation in ToM and pain networks. (B) depicts the movie scenes where higher activation occurred. (B) T1, T2, T3, T4, and T5 represent the ToM scenes with higher activation, whereas P1, P2, P3, P4, and P5 show the pain scenes with higher activation. The movie clips has been taken from original paper<sup>4</sup> and the figure has been recreated.

did not correlate with either the ToM score (Kendall tau correlation test ( $n = 122$ ) :  $rk(120) = 0.005, p = 0.94$ ) or the age (spearman correlation test ( $n = 122$ ) :  $rs(120) = 0.02, p = 0.86$ ). Number of artifact timepoints did not differ between young (3–5 years old) children based on falsebelief task performance (linear regression tests for effect of false belief (FB)-Group on number of motion artifact timepoints: NS effect of FB-group (Pass ( $n = 30$ ) vs. Fail ( $n = 15$ )) :  $b = 0.04, t = 0.12, p = 0.9$ ; NS effect of FB-group (Pass ( $n = 30$ ), Inc ( $n = 20$ ), or Fail ( $n = 15$ )) :  $b < 0.05, p > 0.9$ ) or response inhibition (linear regression test for an effect of Dimensional Change Card Sort task (DCCS) on number of motion artifact timepoints ( $n = 64$ ): NS effect of DCCS summary score:  $b = 0.16, t = 1.18, p = 0.25$ ). We include number of motion artifact timepoints as a covariate in the analysis even though quantity of motion is matched across children and hence probably not driving developmental effects within the child sample. Mean translation, rotation, and distance metrics are strongly linked ( $r > 0.8$ ) with the number of artifact time points.

### Explicit ToM task and false belief composite score and fMRI analysis

In the previous study, six explicit ToM-related questions were administered for the false belief task to identify the correlation between brain development and behavioral scores in ToM reasoning across a wide age range of children<sup>4</sup>. Each child's performance on the ToM-related false belief task was assessed based on the proportion of questions answered correctly out of 24 matched items (14 prediction items and 10 explanation items). Based on the outcome of these explicit false belief task scores, the participants were categorized into three classes: Pass (5–6 correct answers), inconsistent (3–4 correct answers), and fail (0–2 correct answers). In the current study, participants' data were classified in two different ways: (a) into six groups of 3-years, 4-years, 5-years, 7-years, 8–12 years, and adult age groups (reference), and (b) into three false belief tasks outcome-based groups, i.e., pass, inconsistent, and fail. The classification was undertaken to understand the differential developmental changes in the neural activation patterns<sup>26</sup>. Due to the unavailability of data on any 6-years old, that age group could not be added to the above categorization. Further, we computed the magnitude of evoked responses to the events in the movie that evoked peak response magnitude. We selected five time courses ( $> 5$  s) (total no. of time-points = 168), from each network according to the previous study<sup>4</sup>, of maximum activation in ToM (Time-points with maximum activation = 18–27, 82–90, 92–102, 140–149, 150–159) and Pain networks (time-points with maximum activation = 35–49, 78–85, 88–92, 104–115, 159–168) (total of ten time-courses) (refer to Fig. 2, Table 2). The BOLD time series for individual subjects from these groups were extracted from regions of interest (ROIs) anchored in two brain networks—Theory-of-Mind and Pain networks (refer to Table 1). The regions selected for ToM were—bilateral Temporoparietal Junction (LTPJ and RTPJ), posterior cingulate cortex (PCC), Ventro- and dorso-medial prefrontal cortex (vmPFC and dmPFC), and Precuneus, whereas the Pain network regions consist of—bilateral middle frontal gyrus (LMFG and RMFG), bilateral Superior Insula, and bilateral secondary sensory cortex (LSSC and RSSC)<sup>4</sup>. These brain regions and their MNI coordinates were selected from published literature (refer to Table 1)<sup>27,28</sup>. We used the Schaefer atlas for brain parcellation, and by using MNI coordinates, we created a spherical binary mask with a 10 mm radius for all selected ROIs. We extracted time-series for each participant in two ways: (a) from ToM and pain networks separately (6 ROIs each (to check within network variability)) and (b) from both the networks (12 ROIs (to check between-network variability or mixed effect)). Further analyses were carried out on the extracted time series signals.

### BOLD phase coherence and estimation of dynamic functional connectivity

Functional connectivity (FC) is a widely used measure of brain connectivity that quantifies the statistical interdependence between pairs of brain regions over time. FC is estimated from Blood Oxygen Level-Dependent (BOLD) fMRI signals among pairs of brain regions<sup>29–32</sup>. However, these correlation and covariance measures assume that the time series signal for specific brain regions remains static over time, which significantly limits our understanding of whole brain dynamics associated with neurodevelopment. Further temporal changes could carry distinct and meaningful connectivity patterns over the scan and developmental time scales across brain regions<sup>33,34</sup>.

Resting-state data and complex naturalistic stimuli have been shown to encode significant variation among functional brain networks over the entire stimulus duration. Hence, dynamic functional connectivity (DFC) patterns across the whole data set can provide a more penetrating view into the activation patterns over the more commonly used static functional connectivity measure<sup>35</sup>. We have chosen BOLD phase coherence as a measure for the computation of DFC to circumvent the temporal resolution issues that arise in the case of the more popularly employed sliding window correlation method, which is limited by the heuristic selection of the window size. Shorter windows include spurious correlations with high variability and low reliability and have a lower statistical significance due to a lesser number of data points, whereas longer windows are capable

ToM clips description		Pain clips description	
Sr. no.	Description	Sr. no.	Description
T1	Peck flies away to happy cloud	P1	Gus pulls porcupine spines from Peck's head
T2	Peck caught gazing at happy clouds	P2	Alligator biting Peck
T3	Baby crying, then happy	P3	Peck tossing porcupine
T4	Peck dons gear to show why he left	P4	Cloud makes animals (lightning)
T5	Pan from happy clouds to lonely cloud (Gus)	P5	Gus makes alligator (lightning)

**Table 2.** Table showing the selected time-course where higher activation occurred for ToM and pain networks.

of eliminating noise-related correlation while failing to capture significant transient changes in the time series signals<sup>35–38</sup>

Here, we employ BOLD signal phase coherence and quantify the strength of this synchronization while discarding its amplitude. The phase component of the signal sufficiently captures the temporally transient changes, which follows from the observation that two weakly-coupled nonlinear oscillators can synchronize even without any correlation of their amplitudes. Further, phase coherence does not assume stationarity of signals compared to other transformation and coherence-based methods, making this an ideal unsupervised method for characterizing DFC.

Finally, BOLD phase coherence was employed to estimate time-resolved DFC for each subject, resulting in a  $N \times N \times T$  matrix (where  $N = 12$  denotes the number of brain regions and  $T = 168$  represents the total number of time points). To compute the BOLD Phase Coherence, the Hilbert transform was utilized to ascertain the instantaneous phases  $\theta(n, t)$  of the BOLD time series. The modulated BOLD signal  $s(t)$  was then represented analytically using the following equation<sup>14</sup>:

$$z(t) = z_r(t) + jz_i(t) = s(t) + jHT[s(t)], \quad (1)$$

where  $HT[ \cdot ]$  stands for Hilbert Transformation. Using the following formulae, the instantaneous phase  $\theta(t)$  was calculated<sup>14</sup>,

$$\theta(t) = \angle z(t) = \arctan \frac{z_i(t)}{z_r(t)} = \arctan \frac{HT[s(t)]}{s(t)}. \quad (2)$$

DFC ( $n, p, t$ ) was then calculated for the predetermined brain areas  $n$  and  $p$ , as follows<sup>14</sup>:

$$DFC(n, p, t) = \cos(\theta(n, t) - \theta(p, t)). \quad (3)$$

### Computation of dominant dynamic functional connectivity subspaces

Principal components analysis (PCA) is a multivariate, unsupervised dimension reduction technique that separates the data into a set of orthogonal principal components, also known as leading eigenvectors, which are then arranged according to how much variation they contribute to the total variance<sup>39</sup>.

A participant-specific  $DFC(n, p, t)$  matrix of dimension  $N * N$  reflecting the FC between the  $n$ th and  $p$ th brain regions at each time point was subjected to principal component analysis (PCA). As a result,  $DFC(n, p, t)$  or simply  $DFC_t$  may be written as:

$$DFC_t = V^T SV, \quad (4)$$

where  $S$  stands for the diagonal matrix, and  $V$  stands for the leading eigenvector of the  $N \times N$  matrix:

$$\begin{bmatrix} \lambda_1 & \dots & 0 \\ \vdots & \ddots & \vdots \\ 0 & \dots & \lambda_N \end{bmatrix}, \quad \text{such that } \lambda_1 > \lambda_2 > \dots > \lambda_N.$$

The primary components of the DFC are represented by the number of  $k = 3$ . The dominating DFC  $D(n, k, t)$  was calculated as follows:

$$D = \tilde{V}^T \tilde{S} \tilde{V}, \quad (5)$$

where dimensionally reduced matrix is denoted by  $\tilde{V}^T$  and  $\tilde{S}$  is representing diagonal matrix  $\begin{bmatrix} \lambda_1 & \dots & 0 \\ \vdots & \ddots & \vdots \\ 0 & \dots & \lambda_N \end{bmatrix}$ .

Here, we choose  $k = 3$  or three leading eigenvectors that contain 85% information.

### Computation of network temporal stability using dominant DFC subspaces

We characterize the temporal stability of dominant DFC subspaces by estimating their similarity between different time points throughout. Additionally, quantifying the temporal stability of a network over the period of data acquisition can also vouch for the reliability of the connectivity observed and the robustness of the network activity in the face of external disturbances. We used two techniques to achieve that goal: Mahalanobis distance and Angular distance. We used the following equation to determine the distance between DFC sub-spaces from different time points<sup>14</sup>:

1. *Angular distance calculation* Angular distance measures the angle between two vectors or subspaces, which in this study represent dynamic functional connectivity (DFC) patterns at different time points. The angular distance  $\phi(t_x, t_y)$  between two DFC subspaces  $D_{t_x}$  and  $D_{t_y}$  is calculated using the following equation:

$$\phi(t_x, t_y) = \angle(D_{t_x}, D_{t_y}). \quad (6)$$

Here, each entry of the temporal stability matrix  $\phi(t_x, t_y)$  represents the angular separation between the dominant DFC subspaces at time points  $t_x$  and  $t_y$ . The angular distance ranges from 0 to  $\frac{\pi}{2}$ , where  $\frac{\pi}{2}$  denotes high angular distance and 0 denotes low angular distance.  $D_{t_x}$  and  $D_{t_y}$  are matrices of dimensions  $R \times 2$ , where  $R$  represents the number of regions of interest (ROIs) in the brain.

2. *Mahalanobis distance calculation* We estimated the Euclidean distance using the Mahalanobis distance method, which measures the distance between distinct points from one space to another. Mahalanobis distance is defined as a normalised Euclidean distance between a point  $P$  and a distribution  $D$ . In the current study, for each timepoint, Mahalanobis distance was calculated between each brain parcel (ROI) in the reduced dominant dFC subspace  $D_{t_y}$  and complete set of ROIs subspace  $D_{t_x}$ . Every ROI in  $D_{t_y}$  (point P) has Mahalanobis distance estimated with respect to subspace  $D_{t_x}$  (distribution D). Each entry in the temporal stability matrices, thus estimated for each subject, is the Mahalanobis distance averaged across all brain parcels (ROIs). We seek to characterize the temporal stability of the dominant subspaces  $D_t$  by estimating how similar they are across time  $t$ . This was performed for each participant's DFC dominating subspace using the following equation:

$$M^2 = (D_{t_x} - D_{t_y})^T C^{-1} (D_{t_x} - D_{t_y}). \quad (7)$$

Here,  $M^2$  represents the distance between each point. In this equation,  $C$  denotes the covariance matrix, which characterizes the variability and relationships between different dimensions of the data. By taking the inverse of  $C$  ( $C^{-1}$ ), we normalize the distances based on the covariance structure of the data. The resulting Mahalanobis distance matrix provides a measure of similarity between DFC subspaces at different time points.

To ensure that our findings are not confounded by head motion artifacts, we conducted a rigorous analysis to assess the potential impact of motion on the angular and Mahalanobis distances for each sub-group. Following the methodology employed by Richardson et al., we first included motion as a covariate in our regression models to account for any potential motion effects on our distance metrics. For each group, we performed an ordinary least squares (OLS) regression analysis with angular and Mahalanobis distances as the dependent variables and motion as the independent variable. The coefficients, standard errors, t-values, and p-values for the effect of motion were calculated to determine whether motion significantly influenced the observed distances (see Supplementary Material Table S10).

### Validation of results

#### Entropy

To validate results of temporal stability matrices, we calculated entropy that defined measurement of detectable temporal order that we may interpret as the overall stability of the temporal stability matrices<sup>14</sup>. The lower the value of entropy, the higher the stability in the temporal patterns and vice versa. For each subject, we compute the entropy of temporal stability matrices, where each element is the estimated Mahalanobis or Angular distance between the dominant subspaces  $D_{t_x}$  and  $D_{t_y}$ . The entropy was calculated using the following formula<sup>14</sup>:

$$E = -\sum p \log(p), \quad (8)$$

where  $p$  holds the normalized histogram counts.

#### Frobenius norm

Frobenius norm or Euclidean norm of matrix was utilized to quantify the variations between the temporal stability matrices generated for different age groups. We calculated Frobenius norm using the following formula<sup>14</sup>:

$$\|x_F\| = \sqrt{\sum_{i=1}^T \sum_{j=1}^T |a_{ij} - b_{ij}|^2}, \quad (9)$$

where entries of temporal matrices are indicated by  $a_{ij}$  and  $b_{ij}$ .

## Results

### Unsupervised characterization of temporal stability of ToM and pain functional brain networks in 3–12 years age

*Using angular distance to quantify temporal stability differences across different age groups*

To check the distinct temporal stability of ToM and Pain networks at 3–12 years of age, we first calculated angular distance matrices among dominant DFC subspaces identified over all the time points. Subsequently, a  $time \times time$  temporal stability matrix was derived, which was then averaged over all individuals. Each entry in the matrix represented the angle between the dominating DFC subspaces at  $t_x$  and  $t_y$ . As described earlier, we calculated Angular distance into two parts: one for six age categories (3-years to adults) and one for the three false-belief-task performance groups. Figures 3 and 4 represent the subject-average temporal matrices for all 12 ROIs and 6 ROIs in each ToM and Pain network. The higher the value of angular distance, the bigger the leap

between two dominant DFC subspaces at time points  $t_x$  and  $t_y$ . Our results suggested that in terms of capturing temporal stability for defined time courses (For the ToM network (Time-points with maximum activation = 18–27, 82–90, 92–102, 140–149, 150–159) and for pain networks (time-points with maximum activation = 35–49, 78–85, 88–92, 104–115, 159–168) (total of ten time courses)) for all ROIs or, in other words, variability between the networks, we were getting shorter-lived repeated patterns of temporal stability for 3-years and 4-years age groups. Whereas, for other age groups, i.e., 5-years, 7-years, 8–12 years, and adults, we were getting longer-lived temporal stability patterns for defined time courses (refer to Fig. 3). The previous study<sup>4</sup> reported that ToM network segregated as early as 3-years from pain network. To get more insight, we also calculated temporal stability for ToM and pain network separately to check variability within the network. We found longer-lived temporal stability patterns for defined time courses in the ToM network, even for 3-years and 4-years age groups, and it continued till adulthood. Whereas we observed shorter-lived repeated patterns of temporal stability for 3-years and 4-years age groups in pain network and found change in the pattern from 5-year age group (i.e., longer-lived stability pattern) that continued till adulthood. The temporal matrices per age group show higher distance values for All ROIs than the corresponding matrices for ToM or Pain ROIs, and this difference persists through age (refer to Figs. 3, 4, 5, 6).

To quantify differences between temporal matrices, the distance values were converted into Z-scores, and Kolmogorov–Smirnov tests for equality of distributions (all groups were found to have unequal distributions

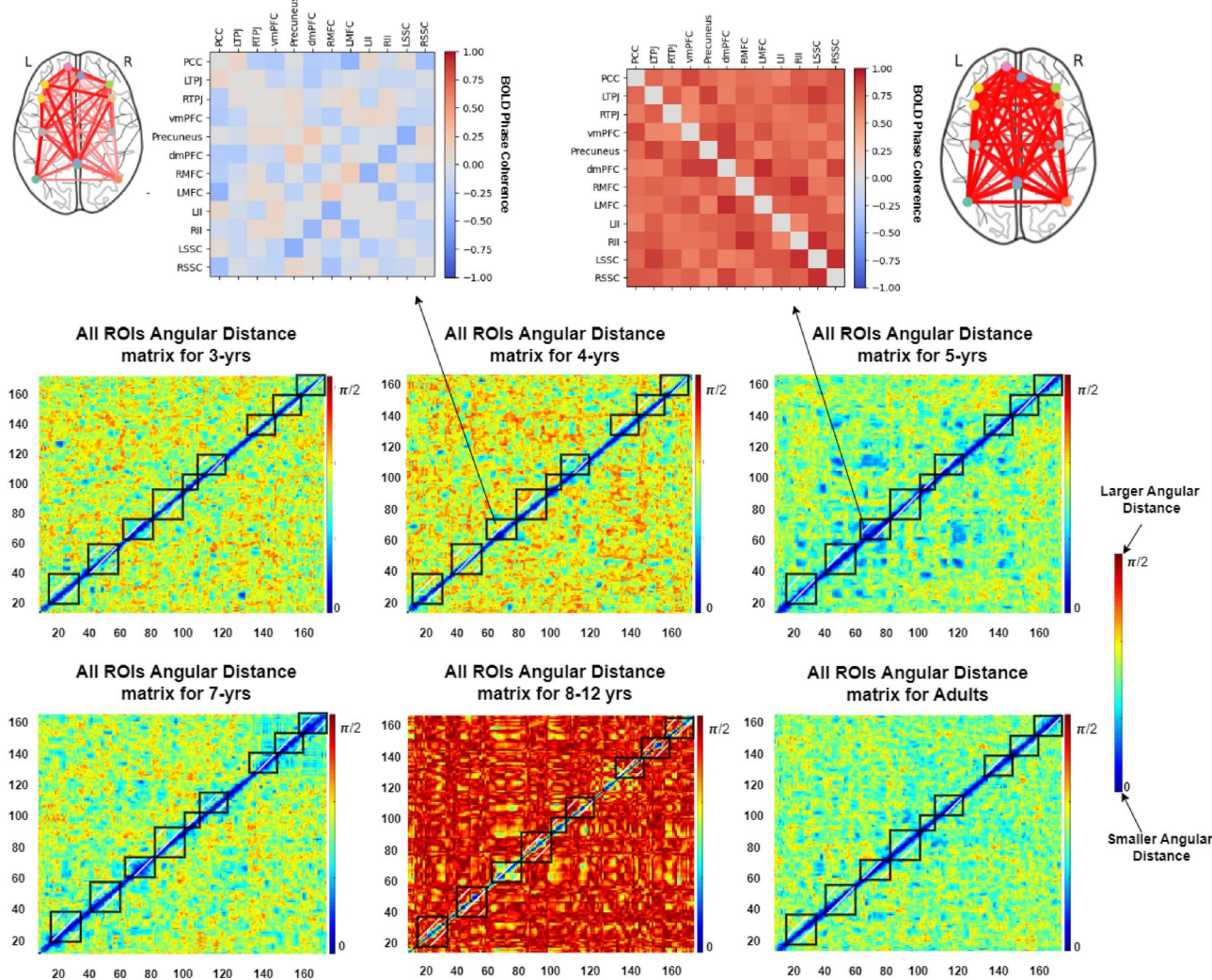


**Figure 3.** Angular distance matrices depicting temporal patterns of all ROIs of the ToM and Pain networks for six age groups (3-years, 4-years, 5-years, 7-years, 8–12 years children and Adults). Each entry in the matrix represents principal angle  $\phi(t_x, t_y)$  between dominant DFC subspaces  $t_x$  and  $t_y$  that ranges from 0 (lower angular distance) to  $\pi/2$  (higher angular distance). Children 3 years and 4 years exhibits shorter-lived larger angular distance values (closer to  $\pi/2$ ), global spread of patterns of temporal stability. On the contrary, 5-years, 7-years, 8–12 years, and adults have low angular distance values (closer to 0) in the matrix and a longer-lived, local spread of stability patterns (indicated by arrows and rectangular boxes). BOLD phase coherence estimated for selective time course of peak activation depicts the differences between dFC patterns estimated for 4- and 5 years age groups.

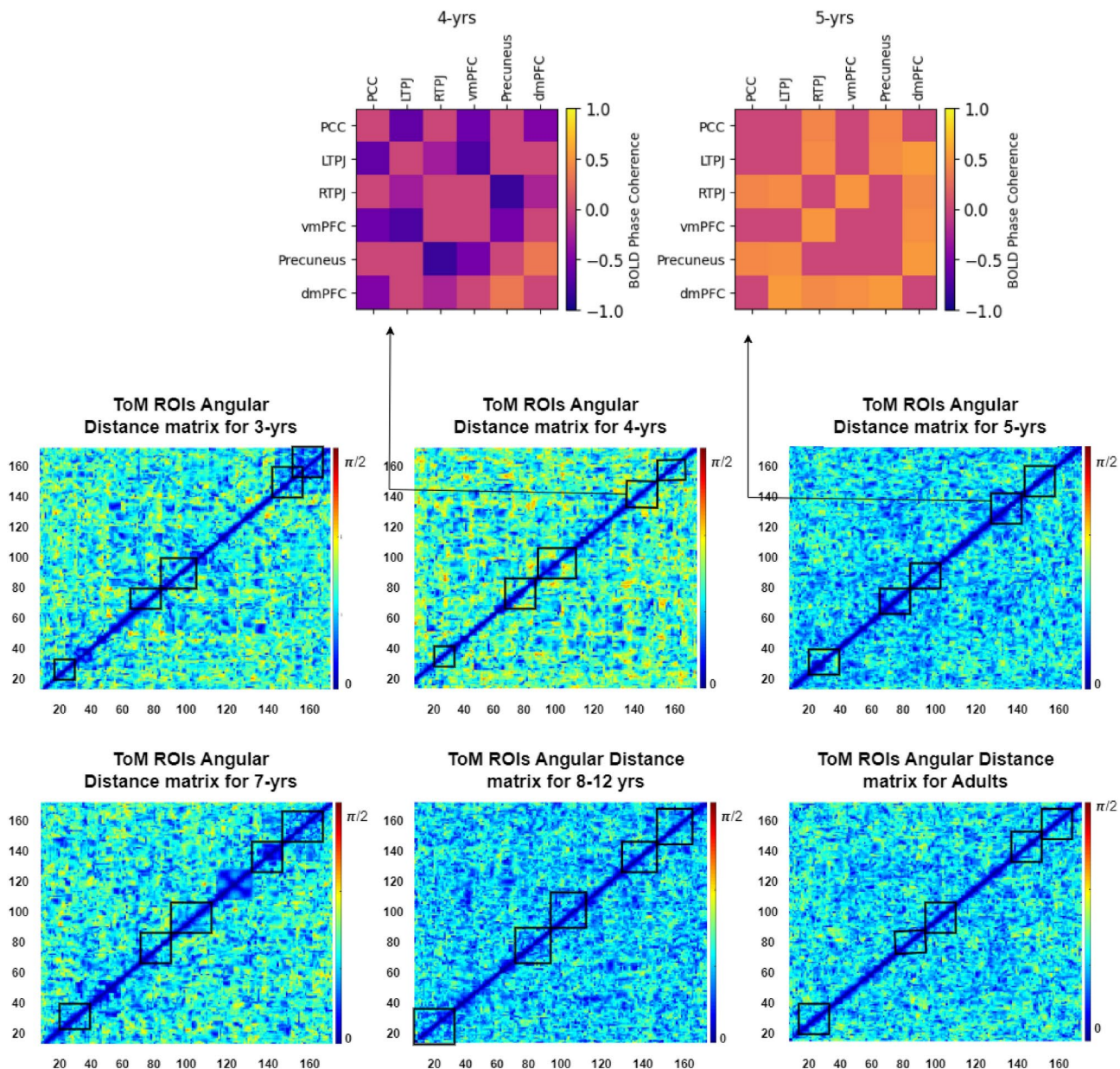


**Figure 4.** Angular distance matrices depicting temporal patterns of ToM network ROIs for each of the six age groups (3, 4, 5, 7, 8–12 years and Adults). BOLD phase coherence is shown for one of the selected timecourse with maximum activation for 4- and 5 years age groups in ToM network (BOLD phase coherence for other timecourses for all six age categories are displayed in Supplementary Fig. S5). We observed longer-lived local spread of smaller angular distance values indicating higher temporal stability patterns for defined time courses in the ToM network for 5-years to adult. Whereas we found shorter-lived higher angular distance values spreaded over the timecourse suggesting global patterns of lower temporal stability and low phase coherence patterns between ToM ROIs for 3-years and 4-years age groups.

with  $p$  varying from  $< 0.4$  to  $< 4 \times 10^{-313}$ ), followed by Kruskal Wallis tests were conducted: All ROIs  $\chi^2(5) = 42.04, p < 6 \times 10^{-8}$ ; Pain ROIs  $\chi^2(5) = 47.63, p < 5 \times 10^{-9}$ ; ToM ROIs  $\chi^2(5) = 24.59, p < 0.0003$ . Dunn–Sidak post-hoc test was performed for pairwise comparisons: All ROIs: 3 years–4 years: diff =  $-1376.4, p = 0.0114$ , 4 years–5 years: diff =  $1716.9, p = 4.8131 \times 10^{-4}$ , 4 years–8 years: diff =  $2212.4, p = 1.3683 \times 10^{-6}$ , 4 years–Adult: diff =  $2004.2, p = 1.9045 \times 10^{-5}$ , 7 years–8–12 years: diff =  $1551.7, p = 0.0025$ , 7 years–Adult: diff =  $1343.6, p = 0.0149$ ; Pain ROIs: 3 years–8–12 years: diff =  $1365.7, p = 0.0125$ , 3 years–Adult: diff =  $1196.6, p = 0.0445$ , 4 years–5 years: diff =  $1735.3, p = 3.9715 \times 10^{-4}$ , 4 years–8–12 years: diff =  $2337.3, p = 2.6373 \times 10^{-7}$ , 4 years–Adult: diff =  $2168.2, p = 2.4350 \times 10^{-6}$ , 7 years–8–12 years: diff =  $1556.7, p = 0.0023$ , 7 years–Adult: diff =  $1387.6, p = 0.0104$ ; ToM ROIs: 3 years–8–12 years: diff =  $1286.6, p = 0.0232$ , 4 years–8–12 years: diff =  $1836.4, p = 1.3342 \times 10^{-4}$ , 4 years–Adult: diff =  $1319.2, p = 0.0180$ , 7 years–8–12 years: diff =  $1302.9, p = 0.0205$ ; rest NS.

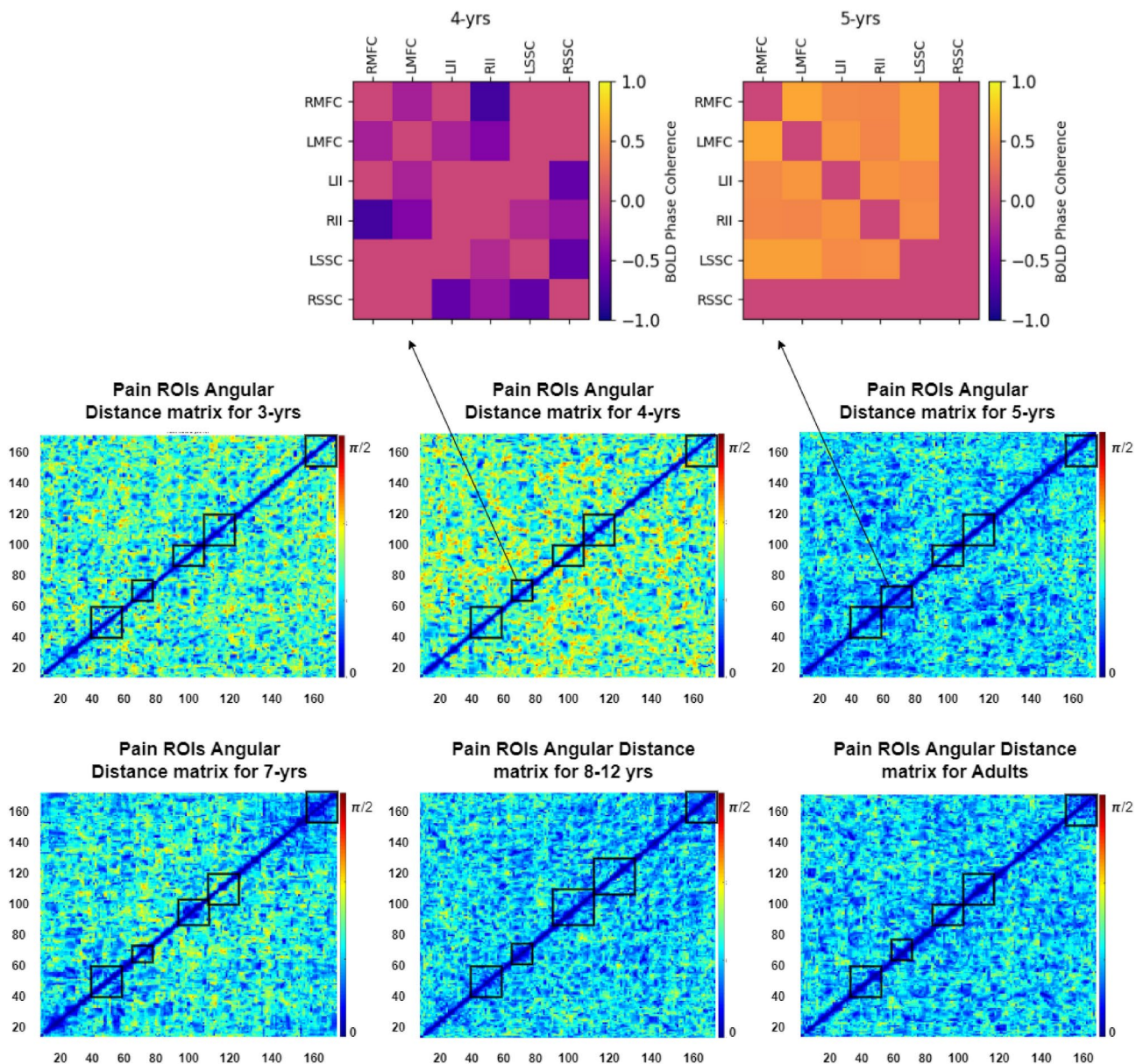


**Figure 5.** Angular distance matrices depicting temporal patterns of pain network ROIs separately for each of the six age groups (3, 4, 5, 7, 8–12 years and Adults) (with maximum activation in pain network for 5 time courses = 35–49, 78–85, 88–92, 104–115, 159–168). We observed longer-lived local spread of temporal stability patterns with low angular distance values for the defined time courses for 5-years to adult suggesting higher temporal stability for extended duration of time and higher phase coherence (for simplicity shown for a single time course 78–85 and remaining time courses are displayed in Supplementary Fig. S5) between brain areas belonging to Pain ROIs. On the contrary, we found shorter-lived higher angular distance values spread over the time course suggesting global patterns of lower temporal stability and low phase coherence patterns between Pain ROIs for 3-years and 4-years age groups.

Entropy was calculated to quantify the complexity of these temporal stability patterns. Figure 6 shows the entropy values calculated from angular distance values for the six age groups as violin plots. In all three graphs (Fig. 6 subgraphs—A, E, F), a higher entropy value is noticed for 4 years compared to the other age groups. A lower entropy value is noticed for 7 years group as compared to the 5 years group, and this corroborates with the qualitative conclusions drawn from the temporal matrices earlier. Kolmogorov–Smirnov test was performed to check for equality of distributions (all groups were found to have unequal distributions with  $p < 0.05$ ), followed by the Kruskal–Wallis tests with non-significant results at 5% confidence level (All ROIs  $\chi^2(5) = 5.54$ ,  $p < 0.4$ ; Pain ROIs  $\chi^2(5) = 10.97$ ,  $p < 0.06$ ; ToM ROIs  $\chi^2(5) = 4.13$ ,  $p < 0.6$ ).

In addition, we computed the Frobenius distance to examine the difference among temporal matrices of ToM and Pain regions (Fig. 4). We find Frobenius distance values to progressively reduce from 3 years to Adults, with

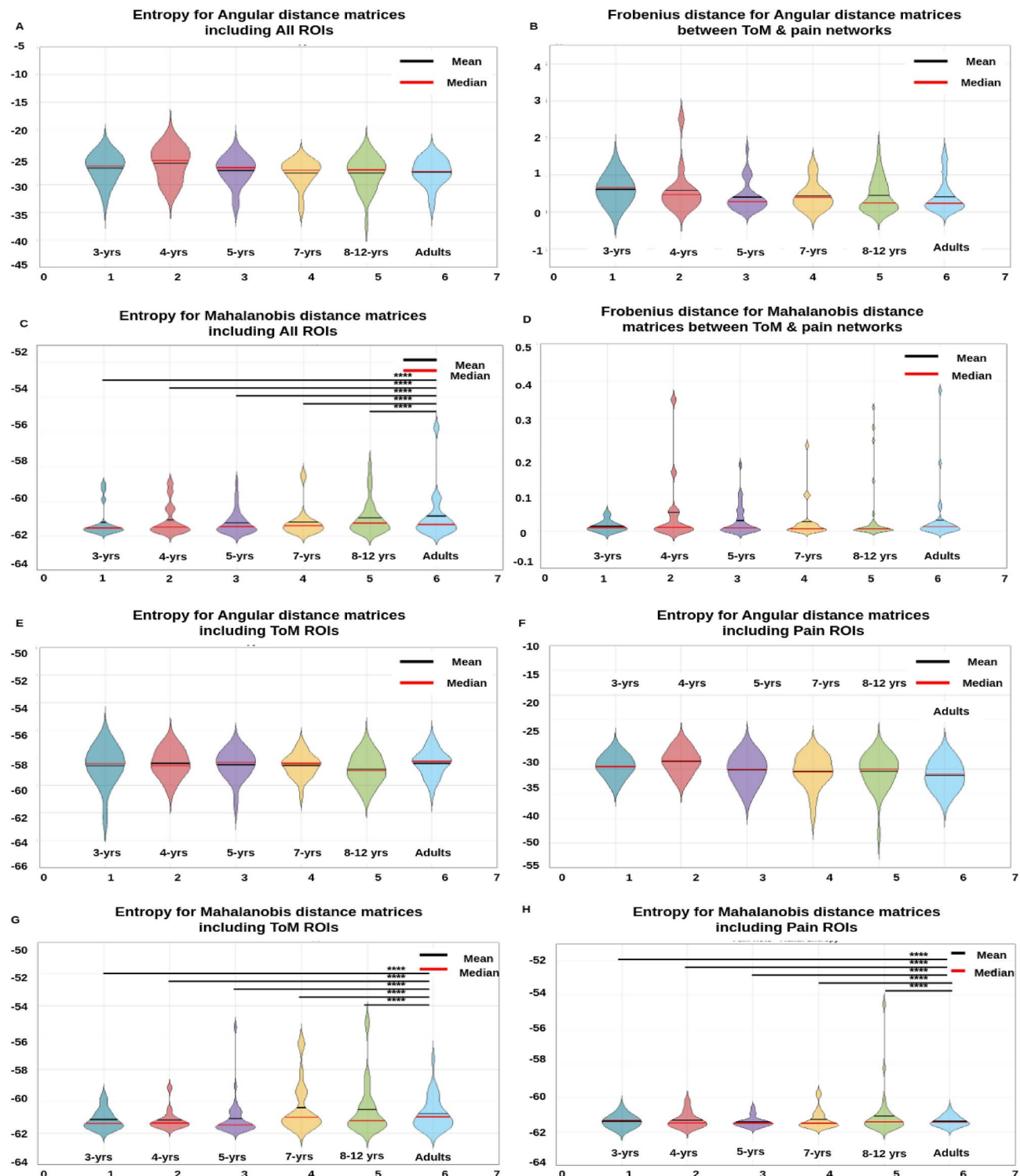


**Figure 6.** Entropy and Frobenius distances matrices: (A,C) are showing entropy for Angular and Mahalanobis distances including All ROIs, whereas (B,D) are depicting Frobenius distance between ToM and Pain ROIs for Angular and Mahalanobis distances. (E–H) are showing entropy for Angular and Mahalanobis distances for ToM and Pain ROIs separately. Statistically significant differences are represented using \*( $P \leq 0.05$ ), \*\* ( $P \leq 0.01$ ), \*\*\* ( $P \leq 0.001$ ), \*\*\*\* ( $P \leq 0.0001$ ), ns (not significant).

an anomalous dip for 5 years. No statistical significance was found using the Kruskal–Wallis test ( $\chi^2(5) = 7.59$ ,  $p < 0.2$ ).

### Using Mahalanobis distance to characterize temporal stability matrices across different age-groups

Next, we estimated the Mahalanobis distance to assess the temporal stability of the DFC. Each matrix element represents the Mahalanobis distance between the dominating DFC subspaces (refer to Supplementary Material Sect. 1). A higher value of Mahalanobis Distance denotes a larger distance between the average of the Euclidean distance between individual ROIs at  $t_x$  and the collection of all ROIs (ToM or Pain network ROIs) at  $t_y$  of the dominant DFC subspaces. We observe shorter-lived repeated patterns of temporal stability for 3-years and 4-years age groups. Consistent with the previous measure, we also find a slight increase in temporal switching dynamics, i.e., longer-lived temporal stability patterns from 5 years to 7 years.

Z-scores were calculated to compare the temporal matrices of these subgroups, Kolmogorov–Smirnov test was performed (all groups were found to have unequal distributions with  $p$  varying from  $< 2 \times 10^{-8}$  to  $< 1 \times 10^{-255}$ ), followed by Kruskal–Wallis (All ROIs  $\chi^2(5) = 18,066.11, p = 0$ ; Pain ROIs  $\chi^2(5) = 3863.9, p = 0$ ; ToM ROIs  $\chi^2(5) = 5254.75, p = 0$ ) and Dunn–Sidak tests (refer to Table 3).

To validate the results, we calculated entropy (shown in Fig. 6), with similar entropy values seen across the age groups, with an exception for ToM ROIs, which display a pattern similar to the observations from the angular distance measure: a higher entropy (and hence more complexity) in 4 years as compared to 3 years, and in 7 years as compared to 5 years. Kolmogorov–Smirnov test was performed to check for equality of distributions (all groups were found to have unequal distributions with  $p < 0.05$ ), followed by the Kruskal Wallis tests (All ROIs  $\chi^2(5) = 72.57, p < 3 \times 10^{-14}$ ; Pain ROIs  $\chi^2(5) = 77.87, p < 2.5 \times 10^{-15}$ ; ToM ROIs  $\chi^2(5) = 82.44, p < 3 \times 10^{-16}$ ) and Dunn–Sidak for the significant results of the six age subgroups (All ROIs: 3 years–Adult: diff =  $-82.5009, p = 3.1472 \times 10^{-8}$ , 4 years–Adult: diff =  $-72.7089, p = 5.6670 \times 10^{-6}$ , 5 years–Adult: diff =  $-77.3391, p = 2.0698 \times 10^{-8}$ , 7 years–Adult: diff =  $-76.595, p = 2.5474 \times 10^{-8}$ , 8–12 years–Adult: diff =  $-64.2068, p = 9.1637 \times 10^{-8}$ ; Pain ROIs: 3 years–Adult: diff =  $-77.9412, p = 1.0955 \times 10^{-7}$ , 4 years–Adult: diff =  $-76.0714, p = 1.6206 \times 10^{-6}$ , 5 years–Adult: diff =  $-81.3824, p = 2.0677 \times 10^{-8}$ , 7 years–Adult: diff =  $-77.0435, p = 2.4449 \times 10^{-8}$ , 8–12 years–adult: diff =  $-74.2941, p = 2.0845 \times 10^{-8}$ ; ToM ROIs: 3 years–Adult: diff =  $-77.1301, p = 1.4829 \times 10^{-7}$ , 4 years–Adult: diff =  $-75.5671, p = 1.9607 \times 10^{-6}$ , 5 years–Adult: diff =  $-83.0419, p = 2.0676 \times 10^{-8}$ , 7 years–Adult: diff =  $-58.8590, p = 2.0455 \times 10^{-5}$ , 8–12 years–Adult: diff =  $064.6889, p = 7.5010 \times 10^{-8}$ ; rest NS) (refer to Table 3).

We also calculated the Frobenius distance between the ToM and Pain network ROIs for the six age subgroups (refer to Fig. 6). We observe a higher distance for 3 years and Adults and a lower distance for all the other age groups. No statistical significance was found using the Kruskal–Wallis test ( $\chi^2(5) = 7.78, p < 0.2$ ).

### Association between performance in false belief task and temporal stability of DFC

Next, we tested our hypothesis that the temporal stability patterns of social brain regions of ToM in 3–12 years could be associated with behavioral scores of the false belief task. Temporal instability was a dominant feature at

Pairs	All ROIs		Pain ROIs		ToM ROIs	
	Difference	p-value	Difference	p-value	Difference	p-value
3 years–4 years	53,917	<b><math>2.0676 \times 10^{-8}</math></b>	4719.4	<b><math>2.0172 \times 10^{-8}</math></b>	23,518	<b><math>2.0693 \times 10^{-8}</math></b>
3 years–5 years	31,162	<b><math>2.1276 \times 10^{-8}</math></b>	-16,415	<b><math>2.0914 \times 10^{-8}</math></b>	-1104.3	0.0818
3 years–7 years	18,966	<b><math>1.0264 \times 10^{-8}</math></b>	-8762	<b><math>2.0472 \times 10^{-8}</math></b>	8240.2	<b><math>2.0216 \times 10^{-8}</math></b>
3 years–8–12 years	24,470	<b><math>2.0676 \times 10^{-8}</math></b>	-9564.9	<b><math>1.9824 \times 10^{-8}</math></b>	-1192.5	0.0458
3 years–Adult	29,884	<b><math>2.7153 \times 10^{-8}</math></b>	-13,855	<b><math>2.9648 \times 10^{-8}</math></b>	6363.1	<b><math>3.5734 \times 10^{-8}</math></b>
4 years–5 years	-22,755	<b><math>2.7859 \times 10^{-8}</math></b>	-21,135	<b><math>4.6713 \times 10^{-8}</math></b>	-24,623	<b><math>2.8327 \times 10^{-8}</math></b>
4 years–7 years	-34,951	<b><math>1.4892 \times 10^{-8}</math></b>	-13481	<b><math>2.7937 \times 10^{-8}</math></b>	-15,278	<b><math>2.6153 \times 10^{-8}</math></b>
4 years–8–12 years	-29,447	<b><math>2.5376 \times 10^{-8}</math></b>	-14,284	<b><math>1.6473 \times 10^{-8}</math></b>	-24,711	<b><math>3.9347 \times 10^{-8}</math></b>
4 years–Adult	-24,033	<b><math>2.0163 \times 10^{-8}</math></b>	-18574	<b><math>2.0672 \times 10^{-8}</math></b>	-17,155	<b><math>2.0748 \times 10^{-8}</math></b>
5 years–7 years	-12,197	<b><math>3.9475 \times 10^{-8}</math></b>	7653.3	<b><math>3.0121 \times 10^{-8}</math></b>	9344.4	<b><math>1.8392 \times 10^{-8}</math></b>
5 years–8–12 years	-6692	<b><math>2.0947 \times 10^{-8}</math></b>	6850.4	<b><math>2.0134 \times 10^{-8}</math></b>	-88.2839	0.9999
5 years–Adult	-1278	<b>0.0247</b>	2560.7	<b><math>2.9612 \times 10^{-8}</math></b>	7467.4	<b><math>2.0632 \times 10^{-8}</math></b>
7 years–8–12 years	5504.7	<b><math>2.6478 \times 10^{-8}</math></b>	-802.8698	0.3779	-9432.7	<b><math>1.9365 \times 10^{-8}</math></b>
7 years–Adult	10,919	<b><math>3.9574 \times 10^{-8}</math></b>	-5092.6	<b><math>1.5384 \times 10^{-8}</math></b>	-1877	<b><math>8.4552 \times 10^{-5}</math></b>
8–12 years–Adult	5414.1	<b><math>5.0253 \times 10^{-8}</math></b>	-4289.7	<b><math>2.7346 \times 10^{-8}</math></b>	7555.7	<b><math>1.8345 \times 10^{-8}</math></b>
Pass–Inc	11,114	<b><math>9.5606 \times 10^{-10}</math></b>	-	-	10,777	<b><math>9.8573 \times 10^{-10}</math></b>
Pass–Fail	2515.5	<b><math>7.7497 \times 10^{-10}</math></b>	-	-	13,537	<b><math>5.8576 \times 10^{-10}</math></b>
Inc–Fail	-8598.4	<b><math>8.8746 \times 10^{-10}</math></b>	-	-	2759.2	<b><math>6.8475 \times 10^{-10}</math></b>

**Table 3.** Table with a difference and p-values calculated using the post-hoc pair-wise Dunn–Sidak test for Mahalanobis distance-derived Z-scores for the six age subgroups (3, 4, 5, 7, 8–12 years and Adult), and for the false belief performance results.

3 and 4 years, but at age 5, we discovered higher temporal stability. We regressed out the age factor and calculated temporal stability for false belief task-based groups. In the current dataset, out of 65 participants (age ranges 3–5 years), 15 participants failed the false belief task. They belonged to 3 years and 4 years age groups, whereas 20 participants were inconsistent during tasks and belonged to mostly 3 years and 4 years and few participants from 5 years. 30 participants passed the task till age 5-years. Approximately all participants passed the task from 5 years age group onward. In our analysis, we focused on children aged 3–5 years for the false-belief task performance, as this age range exhibits significant variability in passing, failing, or inconsistent results. It allows us to better understand the relationship between temporal stability and ToM development without the confounding effect of age. To validate our hypothesis and get more nuanced insight, we performed temporal stability analysis for false belief task performers. For the participants who passed ToM task, their temporal stability was high for ToM network with low angular distance. In contrast, participants who failed the task' temporal stability was low for ToM network with high angular distance (refer to Figs. 7, 8) (refer to Supplementary Material Sect. 2).

*Association between false belief task scores and temporal stability of DFC using angular distance and entropy*  
A qualitative analysis of the angular distance matrices for the false belief task performances reveals longer-lived patterns of temporal stability for pass group when all ROIs and only ToM ROIs were considered, moderate temporal stability patterns for the inconsistent group, and shorter-lived temporal stability patterns for fail group (refer to Fig. 7).

To quantify differences between temporal matrices, the distance values were converted into Z-scores, and Kolmogorov–Smirnov tests for equality of distributions (all groups were found to have unequal distributions with  $p$  varying from  $< 0.4$  to  $< 4 \times 10^{-313}$ ), followed by Kruskal Wallis tests were conducted: All ROIs  $\chi^2(2) = 7.31, p < 0.03$ ; Pain ROIs  $\chi^2(2) = 15.63, p < 0.0005$ ; ToM ROIs  $\chi^2(2) = 12.18, p < 0.003$ . Dunn–Sidak posthoc test was performed for pairwise comparisons: All ROIs: Pass–Fail: diff =  $-533.0409, p = 0.0271$ ; Pain ROIs: Pass–Inc: diff =  $-524.7799, p = 0.0302$ , Pass–Fail: diff =  $-806.1150, p = 2.8977 \times 10^{-4}$ ; ToM ROIs: Pass–Fail: diff =  $-722.1818, p = 0.0014$ ; rest NS.

To quantify the complexity of these temporal stability patterns, entropy was calculated. Kolmogorov–Smirnov test was performed to check for equality of distributions (all groups were found to have unequal distributions with  $p < 0.05$ ), followed by the Kruskal Wallis tests with non-significant results at 5% confidence level (All ROIs  $\chi^2(2) = 1.38, p < 0.6$ ; Pain ROIs  $\chi^2(2) = 2.11, p < 0.4$ ; ToM ROIs  $\chi^2(2) = 2.11, p < 0.8$ ).

*Association between false belief task scores and temporal stability of DFC using Mahalanobis distance and entropy*  
Qualitative analysis of the Mahalanobis distance matrices reveals no differences for the false belief performances (refer to Supplementary Materials Figs. S1, S2).

We calculated Z-scores for comparing the temporal matrices of pass, fail, and inconsistent groups; the Kolmogorov–Smirnov test was performed, followed by Kruskal–Wallis (All ROIs  $\chi^2(2) = 3171.04, p = 0$ ; Pain ROIs  $\chi^2(2) = 5558.54, p = 0$ ; ToM ROIs  $\chi^2(2) = 4777.35, p = 0$ ) and Dunn–Sidak tests (refer to Table 3). We also calculated entropy and found that there is an increasing trend for the false belief test performers, denoting increasing instability from passers to inconsistent performers and failers. To check equality of distribution, we

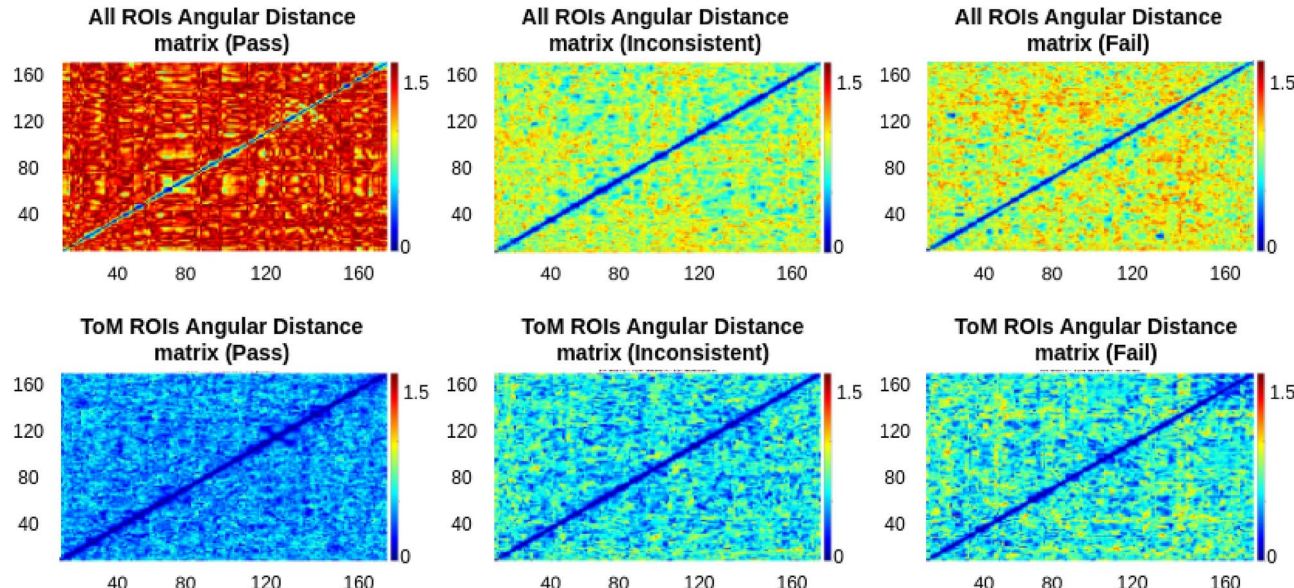


**Figure 7.** Angular distance matrices depicting temporal patterns for a false belief task-based pass, fail, and inconsistent groups. It showed false belief task is dependent on temporal stability. The figure shows higher temporal stability in ToM network for the pass group, moderate stability for the inconsistent group, and lowest temporal stability for the fail group.

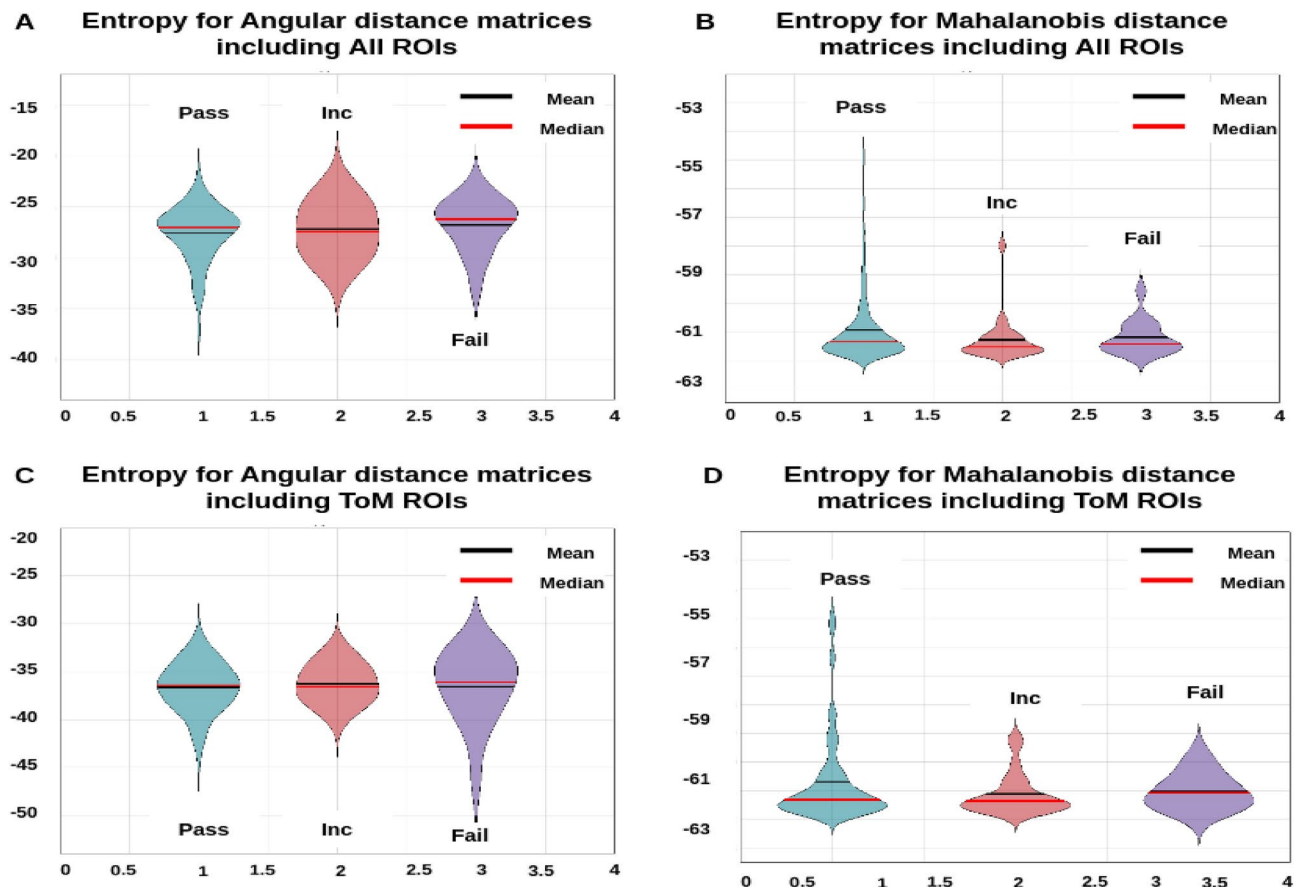


**Figure 8.** (A,C,E) depicts entropy plots for angular distance for the false belief task-based pass, fail, and inconsistent groups. (B,D,F) are depicting entropy plots for Mahalanobis distance. In the case of entropy plots, Mahalanobis distance is better at capturing the differences in temporal stability in different groups.

performed the Kolmogorov–Smirnov test and found all false belief task groups with unequal distribution with  $p < 0.05$  (All ROIs  $\chi^2(2) = 0.61, p < 0.75$ ; Pain ROIs  $\chi^2(2) = 0.57, p < 0.8$ ; ToM ROIs  $\chi^2(2) = 0.71, p < 0.75$ ).

## Discussion

In early life, children's brains and cognitive capacities go through significant changes in the first few years of life. For example, in social cognition, young infants acquire a remarkably sophisticated understanding of others' intentions, ideas, and emotions, as opposed to their physiological effects, sensations, pain, hunger, and body states; a vast majority of this development happens before children begin conventional education at the age of 6 years<sup>4,40–43</sup>. The main objective of this study was to use a naturalistic movie-viewing task that activates the ToM and other functional brain network activations to characterize the temporal stability and fluctuations across developmental age groups specifically for children in the age range of 3–12 years. Using a short, engaging, and naturalistic movie stimulus, functional data was acquired from a large sample of children ( $n = 122$ ), including 65 children between 3 and 5 years of age. The movie stimulus used in this study for DFC analysis of fMRI BOLD signals, Pixar's 'Partly Cloudy,' depicts multiple events that focus on two aspects of the main characters (a cloud named Gus and his stork friend Peck): their bodily sensations (often physical pain) and their mental states (beliefs, desires, and emotions) were salient events that drive developmental change and temporal fluctuations in cortical networks recruited for reasoning about bodies (the pain matrix) and minds (the theory of mind network). Additionally, to identify the age range where reasonable temporal stability was achieved and gradually becoming temporally stable over time (especially for adults). Reasonable temporal stability refers to the point at which DFC patterns show consistent and less fluctuating connectivity states over extended periods, indicating mature and stable brain network functioning. Moreover, we hypothesized that there could be a significant association between the temporal stability of DFC patterns of functional brain networks and the behavioral performance in children across different ages, i.e., temporal stability could be associated with the performance of false belief task-based groups. The participants aged 3 to 12 and adults watched a short animated movie (naturalistic stimuli). The previous study reported that<sup>4</sup>, the movie elicited a significant response from ToM and Pain sensory networks at specific time points, as demonstrated by our results. The dataset was first segmented into 3-years, 4-years, 5-years, 7-years, 8–12 years, and adults to characterize temporal stability differences across ages to address the fluctuation and stochasticity of DFC with development. Subsequently, we used to pass, fail,

and inconsistent groups in the behavioral task to check the association between temporal stability and success in explicit false belief task performance.

### **Stochastic properties of dynamic functional connectivity and age effects in children**

The first hypothesis was to characterize the overlap and distinct patterns of temporal stability of dynamic functional connectivity within ToM and pain functional brain networks in 3–12 years old children and adults. A previous study has employed within- and between-network static functional connectivity analysis to characterize age-associated developmental differences in segregation and integration in ToM and Pain networks in 3–12 years old children<sup>4</sup>. In the present study, we first apply a data-driven, unsupervised approach to characterize the high-dimensional DFC into lower-dimensional patterns by identifying similar dominant FC configurations over certain temporal segments beyond the previously employed methods. Our method allows a stochastic characterization of functional connectivity for salient events in the movie and fluctuation of dynamic configurations over the relevant time points, suggesting segregation and integration of functional brain networks over time. Subsequently, using 2 different measures-Angular and Mahalanobis distances applied on DFCs extracted across time, we capture the stability of DFC through the temporal stability matrices that could be used to draw critical insights about underlying functional brain states. The central idea is that they are considered stable if the dominant FC configurations are similar for extended time points. For empirical validation, we explored modifications in temporal stability matrices across six different age groups: 3-years, 4-years, 5-years, 7-years, 8–12 years, and adults as a control group. For six age subgroups, we employed two methods based on the angular distance and Mahalanobis distance: one included all ROIs (Total of 12); the other took individual networks into account (analysis for ToM and Pain network separately). We found a trend of decreasing angular distance and increasing stability from 3-years to the adults, with 4-years and 7-years showing anomalously higher angular distance and instability in the overall trend, and 5-years exhibiting a pattern similar to that of 8–12 years age group. The increasing stability of higher-cognition and associative brain regions (included in the ToM and Pain networks, respectively) are useful in conferring adaptability and increased capacity to coordinate information processing across the relevant functional networks<sup>12,44–46</sup>. Applying our unsupervised method on movie task-specific brain networks revealed significant differences in temporal stability at different ages during development. Further, It allowed us to identify how ToM network stability patterns at each age shape the age-associated pattern difference. Moreover, our results suggest higher stability, fewer fluctuations, and a capacity to mentalize already developed by the age of 5-years in these children. This trend was not statistically significant in the Mahalanobis Distance measure of DFC patterns due to the presence of outliers. The temporal matrices per age group display higher distance values in global patterns for all ROIs than the corresponding matrices for ToM or Pain ROIs, and this difference persists across increasing age. This could demonstrate the distinctive functioning of ToM and Pain networks from as early as 3-years of age. Finally, we examined the stochastic properties of temporal stability matrices using auto-regressive modeling, motivated by a few recent findings showing dynamic switching between brain networks and time spent visiting distinct brain networks is not random<sup>47,48</sup>. Subsequently, another recent study has shown that the switching dynamics of functional brain states in the resting state follows the AR model of order 1, or in other words, a Markovian process fully explains the DFC evolution when correlation was computed using a sliding window approach<sup>49</sup>. By constructing the unsupervised temporal stability matrices from 2 alternative approaches-principal angle and Mahalanobis distance, we reveal that DFC evolution is neither random nor Markovian.

### **Aging introduces temporal variability in the evolution of dynamic functional connectivity ToM and pain functional brain networks during movie watching**

The previous study<sup>4</sup> reported that the ToM and pain networks are functionally distinct by age 3-years, and functional specialization increases throughout childhood. Recent studies also suggest that DFC of neurocognitive networks in children displays age-related increases in temporal variability of FC among neurocognitive networks. These findings lay the groundwork for understanding how variation in the developing functional network dynamics is related to risk for neurodevelopmental disorders<sup>15,47,49–51</sup>. To compare results with the dynamic fluctuations in the functional brain networks during development we quantified temporal matrices for all 12 and 6 ROIs anchored in ToM and Pain functional brain networks. The higher the value of angular distance, the bigger the leap between two dominant DFC subspaces at different time points  $t_x$  and  $t_y$ . Temporal stability results for defined time courses (for ToM network (Time-points with maximum activation = 18–27, 82–90, 92–102, 140–149, 150–159) and pain networks (time points with maximum activation = 35–49, 78–85, 88–92, 104–115, 159–168) (total of ten time-courses)) for all ROIs, capturing variability between these functional networks. We discovered shorter-lived repeated patterns of temporal stability for 3-years and 4-years age groups. In contrast, for other age groups, i.e., 5-years, 7-years, 8–12 years, and adults, we found longer-lived temporal stability patterns for defined time courses suggesting an age-associated increase in temporal stability and lesser transient switching of functional connectivity patterns. These results complement prior studies in adults that suggest that ToM brain region selectivity increases with age. To get further insight, we also calculated temporal stability for ToM and pain network separately to check variability within the network. We found longer-lived temporal stability patterns for defined time courses in the ToM network, even for 3-years and 4-years age groups, and it continued till adulthood. We observed shorter-lived repeated patterns of temporal stability for 3-years and 4-years age groups in the pain network. We found a change in the stability pattern from the 5-years age group (i.e., longer-lived stability pattern) that continued till adulthood. The temporal matrices per age group show higher distance values for All ROIs than the corresponding matrices for ToM or Pain ROIs, and this difference persists through age. Our results for 3-years and 4-years age groups complement previous findings reporting regions in these two networks were uncorrelated based on FC in the 3-years old; however, they were robustly anti-correlated in older children and adults (FC of ToM and Pain matrix). Change in the temporal stability

patterns from the 5-years group predicted the maturity (i.e., similarity to adults) of each network's distinct temporal fluctuations evoked by the specific movie clips highlighted by time points with maximum activation.

During validation of results using Frobenius Distance analysis, we find the lowest distance between ToM and Pain network activation patterns for 7-years, followed by moderately lower values for 5-years, 8–12-years, and Adults, with high Frobenius Distance value for 3-years, and the highest value for 4 years. Frobenius norm was used to measure the differences between the temporal stability matrices computed for ToM and Pain networks. Hence, higher Frobenius norms in 3 and 4-years compared with 5-years, 7-years, 8–12 years, and adults argue for developmental differences in ToM and Pain networks. ToM and Pain networks' temporal stability of DFC patterns are more similar between 5-years, and adults predicted the maturity (i.e., similarity to adults).

### **Association between performance on false belief tasks in children and temporal stability of DFC in ToM functional brain networks**

The second major goal of this study was to ask how the temporal stability of DFC patterns in the ToM network relates to children's theory of mind cognitive abilities. In this context, the behavioural data used in this analysis comprises questions about other people's actions, beliefs, desires, expectations, and moral blameworthiness. Within this set of questions, six focused on predicting and explaining actions based on false beliefs. Compared to the previous fMRI studies of ToM, the sample included in this paper had a substantial number of children who systematically failed explicit false belief tests. Hence, this allowed us to test for signatures of temporal stability of DFC of specific functional brain networks that were associated with improved performance on false-beliefs tasks. For the false belief performance groups, a lower distance and higher repeatability in patterns were observed for passers, with increasing distances and instability observed for those who failed. Our results are consistent with previous findings that passing false belief tasks was associated with increased functional correlations among regions in the ToM network. This further suggests that increased functional correlations in the ToM network may drive the stability of DFC patterns and may be associated with age. This contrasts with previous findings focusing specifically on 3- to 5-years old children, reporting that the neural responses are very similar to social movies in children who systematically fail versus pass explicit false belief tasks. However, our dynamic FC analysis captured subtle variations and nuanced findings that were missed by previous analyses.

Our results are consistent with the existing literature, as at the early childhood stage, ToM and other networks are still developing, and hence, their temporal stability is low. Gradually, these networks become stable with increasing age. The participants who failed the false-beliefs tasks belonged to 3 years and 4 years groups indexed by lower temporal stability. Interestingly, 3-years old children who systematically failed false belief tasks recruited ToM brain regions at time points with maximum activation in the movie and as a distinct network from the pain matrix. At the same time, the participants who passed mostly belonged to the 5-years age group, where we observed reasonable temporal stability. To get more clarity, we separately performed temporal stability analysis for pass, inconsistent, and fail groups and observed higher temporal stability for the pass group, moderate temporal stability for the inconsistent group, and low temporal stability for the fail group.

### **Conclusion**

In this research, we proposed an architecture to examine the developmental changes in temporal stability of ToM and pain networks using a dynamic functional connectivity approach throughout childhood to adolescence. The outcomes of the study suggested that ToM network gets temporal stability at age of 3 years, whereas more reasonable temporal stability is at age of 5 years, and same pattern for pain sensory network. We were getting more temporal stability for ToM and pain networks for some particular time points where activation was very high. Brain networks are not properly segregated from each other at early childhood stage, it gets more specialized over time. According to our observation, this might be the reason why we were getting low temporal stability at early childhood stage. The current findings are novel, as there is no such method in which temporal stability has been calculated from the early childhood stage, as well as could also be associated with the behavior of the false belief task. There are a few significant limitations of this study which are as follows: (1) Size of dataset; we used a dataset that contained 155 subjects. In the future, we will include dataset with large no. of samples with different tasks. (2) Tested proposed architecture only in healthy participants. In the future, we will try to include participants suffering from neurological disorders (like autism, ADHD, etc.), so might be some correlation that remained an open question for future.

### **Data availability**

Unsupervised characterization of the DFC matrix and stability calculations will be made available on GitHub: <https://github.com/dynamicdip/>. The pipeline for the Analysis of Connectomes (SPM8), including slice-time correction, motion correction, functional normalization, and smoothing procedure on the movie-watching dataset, including T1 and T2 images of fMRI data. The datasets generated during the analysis pipelines in the present study are available from the corresponding author upon reasonable request. The codes for all the analyses carried out in this paper are also available at <https://bitbucket.org/cbdl/workspace/projects/DFC>.

Received: 13 January 2024; Accepted: 11 September 2024

Published online: 28 September 2024

### **References**

- Westby, C. & Robinson, L. A developmental perspective for promoting theory of mind. *Top. Lang. Disord.* **34**, 362–382 (2014).
- Bhavna, K., Banerjee, R. & Roy, D. End-to-end explainable AI: Derived theory-of-mind fingerprints to distinguish between autistic and typically developing and social symptom severity. *BioRxiv* **1**, 1 (2023).

3. Devine, R. T. & Apperly, I. A. Willing and able? Theory of mind, social motivation, and social competence in middle childhood and early adolescence. *Dev. Sci.* **25**, e13137 (2022).
4. Richardson, H., Lisandrelli, G., Riobueno-Naylor, A. & Saxe, R. Development of the social brain from age three to twelve years. *Nat. Commun.* **9**, 1–12 (2018).
5. Astington, J. W. & Edward, M. J. The development of theory of mind in early childhood. *Encycl. Early Childhood Dev.* **14**, 1–7 (2010).
6. Bartsch, K. & Wellman, H. M. *Children Talk About the Mind* (Oxford University Press, 1995).
7. Fair, D. A. et al. Functional brain networks develop from a “local to distributed” organization. *PLoS Comput. Biol.* **5**, e1000381 (2009).
8. Gu, S. et al. Emergence of system roles in normative neurodevelopment. *Proc. Natl. Acad. Sci.* **112**, 13681–13686 (2015).
9. Dosenbach, N. U. et al. Prediction of individual brain maturity using fmri. *Science* **329**, 1358–1361 (2010).
10. Satterthwaite, T. D. et al. Heterogeneous impact of motion on fundamental patterns of developmental changes in functional connectivity during youth. *Neuroimage* **83**, 45–57 (2013).
11. Kana, R. K. et al. Aberrant functioning of the theory-of-mind network in children and adolescents with autism. *Mol. Autism* **6**, 1–12 (2015).
12. Li, L., Lu, B. & Yan, C.-G. Stability of dynamic functional architecture differs between brain networks and states. *Neuroimage* **216**, 116230 (2020).
13. Zhang, J. et al. Neural, electrophysiological and anatomical basis of brain-network variability and its characteristic changes in mental disorders. *Brain* **139**, 2307–2321 (2016).
14. Sastry, N. C., Roy, D. & Banerjee, A. Stability of sensorimotor network sculpts the dynamic repertoire of resting state over lifespan. *Cereb. Cortex* **33**, 1246 (2022).
15. Harlalka, V., Bapi, R. S., Vinod, P. & Roy, D. Atypical flexibility in dynamic functional connectivity quantifies the severity in autism spectrum disorder. *Front. Hum. Neurosci.* **13**, 6 (2019).
16. Dufour, N. et al. Similar brain activation during false belief tasks in a large sample of adults with and without autism. *PLoS ONE* **8**, e75468 (2013).
17. Bruneau, E. G., Jacoby, N. & Saxe, R. Empathic control through coordinated interaction of amygdala, theory of mind and extended pain matrix brain regions. *Neuroimage* **114**, 105–119 (2015).
18. Reher, K. & Sohn, P. Partly cloudy. In *Motion Picture (Pixar Animation Studios and Walt Disney Pictures, 2009)* (2009).
19. Keil, B. et al. Size-optimized 32-channel brain arrays for 3 t pediatric imaging. *Magn. Reson. Med.* **66**, 1777–1787 (2011).
20. Penny, W. D., Friston, K. J., Ashburner, J. T., Kiebel, S. J. & Nichols, T. E. *Statistical Parametric Mapping: The Analysis of Functional Brain Images* (Elsevier, 2011).
21. Cantlon, J. F., Brannon, E. M., Carter, E. J. & Pelpfrey, K. A. Functional imaging of numerical processing in adults and 4-y-old children. *PLoS Biol.* **4**, e125 (2006).
22. Burgund, E. D. et al. The feasibility of a common stereotactic space for children and adults in fmri studies of development. *Neuroimage* **17**, 184–200 (2002).
23. Whitfield-Gabrieli, S., Nieto-Castanon, A. & Ghosh, S. Artifact detection tools (art). *Cambridge MA Release Version 7*, 11 (2011).
24. Richardson, H. & Saxe, R. Development of predictive responses in theory of mind brain regions. *Dev. Sci.* **23**, e12863 (2020).
25. Richardson, H., Saxe, R. & Bedny, M. Neural correlates of theory of mind reasoning in congenitally blind children. *Dev. Cogn. Neurosci.* **63**, 101285 (2023).
26. Huitt, W. & Hummel, J. Piaget’s theory of cognitive development. *Educ. Psychol. Interact.* **3**, 1–5 (2003).
27. Mazziotta, J. C. et al. A probabilistic atlas of the human brain: Theory and rationale for its development. *Neuroimage* **2**, 89–101 (1995).
28. Mazziotta, J. et al. A probabilistic atlas and reference system for the human brain: International consortium for brain mapping (icbm). *Philos. Trans. R. Soc. Lond. Ser. B Biol. Sci.* **356**, 1293–1322 (2001).
29. Friston, K. J., Frith, C. D., Liddle, P. F. & Frackowiak, R. S. Functional connectivity: The principal-component analysis of large (pet) data sets. *J. Cereb. Blood Flow Metab.* **13**, 5–14 (1993).
30. Biswal, B., Zerrin Yetkin, F., Haughton, V. M. & Hyde, J. S. Functional connectivity in the motor cortex of resting human brain using echo-planar mri. *Magn. Reson. Med.* **34**, 537–541 (1995).
31. Friston, K. J. Functional and effective connectivity: A review. *Brain Connect.* **1**, 13–36 (2011).
32. Gaudet, I., Hüller, A., Vannasing, P. & Gallagher, A. Functional brain connectivity of language functions in children revealed by EEG and MEG: A systematic review. *Front. Hum. Neurosci.* **14**, 62 (2020).
33. Chang, C. & Glover, G. H. Time-frequency dynamics of resting-state brain connectivity measured with fmri. *Neuroimage* **50**, 81–98 (2010).
34. Menon, S. S. & Krishnamurthy, K. A comparison of static and dynamic functional connectivities for identifying subjects and biological sex using intrinsic individual brain connectivity. *Sci. Rep.* **9**, 1–11 (2019).
35. Hutchison, R. M. et al. Dynamic functional connectivity: Promise, issues, and interpretations. *Neuroimage* **80**, 360–378 (2013).
36. Glerean, E., Salmi, J., Lahnakoski, J. M., Jääskeläinen, I. P. & Sams, M. Functional magnetic resonance imaging phase synchronization as a measure of dynamic functional connectivity. *Brain Connect.* **2**, 91–101 (2012).
37. Hutchison, R. M., Womelsdorf, T., Gati, J. S., Everling, S. & Menon, R. S. Resting-state networks show dynamic functional connectivity in awake humans and anesthetized macaques. *Hum. Brain Mapp.* **34**, 2154–2177 (2013).
38. Preti, M. G., Bolton, T. A. & Van De Ville, D. The dynamic functional connectome: State-of-the-art and perspectives. *Neuroimage* **160**, 41–54 (2017).
39. Cabral, J. et al. Cognitive performance in healthy older adults relates to spontaneous switching between states of functional connectivity during rest. *Sci. Rep.* **7**, 5135 (2017).
40. Schult, C. A. & Wellman, H. M. Explaining human movements and actions: Children’s understanding of the limits of psychological explanation. *Cognition* **62**, 291–324 (1997).
41. Schulz, L. E., Bonawitz, E. B. & Griffiths, T. L. Can being scared cause tummy aches? Naïve theories, ambiguous evidence, and preschoolers’ causal inferences. *Dev. Psychol.* **43**, 1124 (2007).
42. Cohen, E., Burdett, E., Knight, N. & Barrett, J. Cross-cultural similarities and differences in person-body reasoning: Experimental evidence from the United Kingdom and Brazilian Amazon. *Cogn. Sci.* **35**, 1282–1304 (2011).
43. van Buuren, M. et al. Intrinsic network interactions explain individual differences in mentalizing ability in adolescents. *Neuropsychologia* **151**, 107737 (2021).
44. Cole, M. W., Pathak, S. & Schneider, W. Identifying the brain’s most globally connected regions. *Neuroimage* **49**, 3132–3148 (2010).
45. Yuan, Y. et al. Distinct dynamic functional connectivity patterns of pain and touch thresholds: A resting-state fmri study. *Behav. Brain Res.* **375**, 112142 (2019).
46. Dehaene, S., Lau, H. & Kouider, S. What is consciousness, and could machines have it? *Robot. AI Hum. Sci. Ethics Policy* **1**, 43–56 (2021).
47. Marusak, H. A. et al. Dynamic functional connectivity of neurocognitive networks in children. *Hum. Brain Mapp.* **38**, 97–108 (2017).
48. Vidaurre, D., Smith, S. M. & Woolrich, M. W. Brain network dynamics are hierarchically organized in time. *Proc. Natl. Acad. Sci.* **114**, 12827–12832 (2017).

49. Liegeois, R., Laumann, T. O., Snyder, A. Z., Zhou, J. & Yeo, B. T. Interpreting temporal fluctuations in resting-state functional connectivity mri. *Neuroimage* **163**, 437–455 (2017).
50. White, T. & Calhoun, V. D. Dissecting static and dynamic functional connectivity: Example from the autism spectrum. *J. Exp. Neurosci.* **13**, 1179069519851809 (2019).
51. Roy, D. & Uddin, L. Q. Atypical core-periphery brain dynamics in autism. *Netw. Neurosci.* **5**, 295–321 (2021).

## Acknowledgements

We acknowledge the generous support of IIT Jodhpur Core funds and the Computing facility. D.R. acknowledges the generous support of the NBRC Flagship program BT/MEDIII/NBRC/Flagship/Program/2019: Comparative mapping of common mental disorders (CMD) over the lifespan.

## Author contributions

Km Bhavna and DR were involved in the primary study design, and Km Bhavna, DR, and RB were involved in the planned conceptual analysis. Km Bhavna analyzed data, and Nivava Ghosh helped her with data analysis. DR and RB were mainly responsible for the supervision and funding of this study, Km Bhavna, RB, and DR all contributed to writing this original research article.

## Competing interests

The authors declare no competing interests.

## Additional information

**Supplementary Information** The online version contains supplementary material available at <https://doi.org/10.1038/s41598-024-72945-4>.

**Correspondence** and requests for materials should be addressed to D.R.

**Reprints and permissions information** is available at [www.nature.com/reprints](http://www.nature.com/reprints).

**Publisher's note** Springer Nature remains neutral with regard to jurisdictional claims in published maps and institutional affiliations.

**Open Access** This article is licensed under a Creative Commons Attribution-NonCommercial-NoDerivatives 4.0 International License, which permits any non-commercial use, sharing, distribution and reproduction in any medium or format, as long as you give appropriate credit to the original author(s) and the source, provide a link to the Creative Commons licence, and indicate if you modified the licensed material. You do not have permission under this licence to share adapted material derived from this article or parts of it. The images or other third party material in this article are included in the article's Creative Commons licence, unless indicated otherwise in a credit line to the material. If material is not included in the article's Creative Commons licence and your intended use is not permitted by statutory regulation or exceeds the permitted use, you will need to obtain permission directly from the copyright holder. To view a copy of this licence, visit <http://creativecommons.org/licenses/by-nc-nd/4.0/>.

© The Author(s) 2024